Inversion of Axial Coordination in Myoglobin to Create a "Proximal" Ligand Binding Pocket†

Tadayuki Uno,*,‡ Rikiharu Sakamoto,‡ Yoshikazu Tomisugi,‡ Yoshinobu Ishikawa,‡ and Anthony J. Wilkinson§

Graduate School of Pharmaceutical Sciences, Kumamoto University, Oehonmachi, Kumamoto 862-0973, Japan, and Structural Biology Laboratory, Department of Chemistry, University of York, Heslington, York YO10 5DD, United Kingdom

Received April 10, 2003; Revised Manuscript Received July 5, 2003

ABSTRACT: A ligand binding pocket has been created on the proximal side of the heme in porcine myoglobin by site-directed mutagenesis. Our starting point was the H64V/V68H double mutant which has been shown to have bis-histidine (His68 and His93) heme coordination [Dou, Y., Admiraal, S. J., Ikeda-Saito, M., Krzywda, S., Wilkinson, A. J., Li, T., Olson, J. S., Prince, R. C., Pickering, I. J., George, G. N. (1995) *J. Biol. Chem. 270*, 15993−16001]. The replacement of the proximal His93 ligand by noncoordinating Ala (H64V/V68H/H93A) or Gly (H64V/V68H/H93G) residues resulted unexpectedly in a six-coordinate low-spin species in both ferric and ferrous states. To test the hypothesis that the sixth coordinating ligand in the triple mutants was the imidazole of His97, this residue was mutated to Phe, in the quadruple mutants, H64V/V68H/H93A/H97F and H64V/V68H/H93G/H97F. The ferric quadruple mutants show a clear water/hydroxide alkaline transition and high cyanide and CO affinities, characteristics similar to those of wild-type myoglobin. The ν(Fe−CO) and ν(C−O) stretching frequencies in the ferrous-CO state of the quadruple mutants indicate that the "proximal" ligand binding heme pocket is less polar than the distal pocket in the wild-type protein. Thus, we conclude that the proximal heme pocket in the quadruple mutants has a similar affinity for exogenous ligands to the distal pocket of wild-type myoglobin but that the two pockets have different polarities. The quadruple mutants open up new approaches for developing heme chemistry on the myoglobin scaffold.

Myoglobin (Mb)[1] is a heme-containing oxygen storage protein which has been the subject of intense research over the last few decades. Its robust globin fold and the facility with which it can be purified in recombinant form from *Escherichia coli* expression systems (*1*−*3*) have made Mb an attractive target for protein engineering (*4*). The heme iron is coordinated to the protein through the "proximal" histidine-93 (F8), and the oxygen molecule binds to the axial coordination site on the opposite, "distal" face of the heme. Several amino acid residues in the distal heme pocket of Mb are highly conserved across species (*5*, *6*), prominent among which is the distal histidine-64 (E7) which both stabilizes the bound oxygen through the formation of a hydrogen bond (*7*, *8*) and inhibits autoxidation of the heme iron (*9*).

The functional contributions of many of the distal pocket residues have been probed using site-directed mutagenesis (*4*). Mutations of the conserved Phe CD1, Val E11, Leu B10, and His E7 greatly perturb both the affinity of Mb for exogenous ligands and the stability of the heme (*10*, *11*). Through combined structure−function studies of scores of mutant Mbs, it has been established that displacement of a noncoordinated water molecule from the distal pocket of deoxyMb is a significant barrier to ligand binding to the ferrous heme (*7*, *12*). A water molecule is also stabilized in the ferric protein through direct coordination to the iron atom and hydrogen bonding to His E7 (*12*, *13*). Replacement of His E7 with Leu or Val creates an apolar pocket, resulting in loss of these waters (*12*). Val occurs naturally at position E7 in *Aplysia* Mb; however, in this case Arg E10 is believed to fold back into the pocket so that the guanidinium group makes favorable interactions with bound oxygen (*14*, *15*). These experiments establish that the polarity of the distal heme pocket is a key determinant of ligand affinity (*16*).

We have reported previously that the heme iron in an H64V/V68H (VH) double mutant of pig Mb, in which the distal His64 (E7) and Val68 (E11) are exchanged, is six-coordinate, the imidazole groups of His68 and His93 (F8) forming the two axial ligands. The VH crystal structure shows that the plane of the imidazole ring of His68 is tilted relative to the heme normal and that it is not parallel to that of His93 (Figure 1). His68 is a weaker ligand than His93, as evidenced by the population of the ferric high-spin state at ambient temperatures (*17*) and the longer Fe−His68 bond (*18*). This weaker bonding may be attributed to the less extensive overlap of the bonding orbitals of Nϵ of His68 and those of the iron, as a result of the distorted His68 coordination geometry. The overall structures of ferric VH

† This work is supported in part by a grant for Health Sciences Research on Advanced Medical Technology (H10-Blood-003 to T.U.) from the Ministry of Health and Welfare, Japan. A.J.W. is supported by the BBSRC, U.K.

* Corresponding author. Telephone and fax: +81-96-371-4350. E-mail: unot@gpo.kumamoto-u.ac.jp.

‡ Kumamoto University.

§ University of York.

[1] Abbreviations: Mb, myoglobin; VH, H64V/V68H double mutant; VHA, H64V/V68H/H93A triple mutant; VHG, H64V/V68H/H93G triple mutant; VHAF, H64V/V68H/H93A/H97F quadruple mutant; VHGF, H64V/V68H/H93G/H97F quadruple mutant.

10.1021/bi034569z CCC: $25.00
Published on Web 07/31/2003

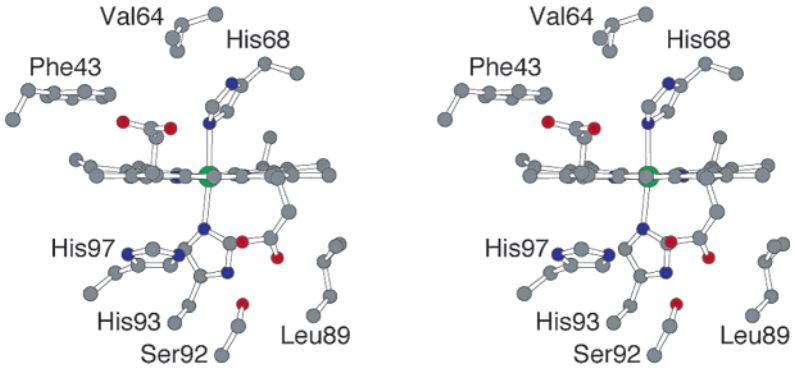

FIGURE 1: Residues surrounding the heme in H64V/V68H (VH) Mb. The figure was drawn using the atomic coordinate set 1MNI.pdb (*18*). The coloring is by atom type: C (grey), O (red), N (blue), and Fe (green).

and wild-type (WT) Mb are otherwise closely similar, and side chain rearrangements are restricted to the heme vicinity.

The creation of a ligand binding pocket on the proximal side of the heme is challenging because mutations of the proximal histidine in WT Mb normally have serious effects on protein expression and stability, a problem that has been overcome in part by growing cells expressing an H93G mutant on media supplemented with imidazole. The latter stabilizes the mutant protein by effectively replacing the proximal histidine. This proximal imidazole ligand can subsequently be replaced by other large nitrogen- and sulfur-based ligands (*19*−*22*). We reasoned that such a pocket might be easier to construct in the VH double mutant, as heme loss is expected to be inhibited by His68 coordination to the heme iron on the distal side. A proximal pocket created in this way would provide a more robust framework for subsequent protein engineering. This is because, unlike the E-helix which forms a prominent component of the distal pocket, the F-helix which shapes the proximal face of the heme is not a key determinant of apoglobin stability (*23*). As a result, Mb is likely to be more tolerant of polar substitutions, usually needed to introduce reactivity, on the proximal side.

To create a proximal heme pocket, we first constructed triple mutants of porcine Mb in which the proximal His93 is replaced by Gly (H64V/V68H/H93G, VHG) or Ala (H64V/V68H/H93A, VHA), which have noncoordinating and less bulky side chains. These mutants were unexpectedly found to exist as six-coordinated low-spin ferric and ferrous species, suggesting two strong-field ligands at the axial positions. To explore the possibility that His97 (FG1) was coordinating the iron in the triple mutants, we replaced this residue by Phe, creating H64V/V68H/H93G/H97F, VHGF; and H64V/V68H/H93A/H97F, VHAF. These quadruple mutants exhibited a number of spectral properties similar to WT Mb. Thus, a "proximal" heme pocket has been constructed successfully on a Mb scaffold. Since a heme pocket is a prerequisite for ligand binding, these mutants set a new stage for exploiting heme chemistry.

MATERIALS AND METHODS

Preparation of Mb Mutants. A pBluescriptII KS(+) (Stratagene) plasmid derivative harboring the coding sequence for the porcine VH Mb double mutant was used as a template for mutagenesis. Site-directed mutagenesis was performed using the QuikChange system (Stratagene), and the mutated plasmids were used to transform *E. coli* XL-1 Blue MRF′ (Stratagene). The presence of the mutations was confirmed by DNA sequencing (Li-Cor Model 4200S2 DNA sequencer). *Bam*HI/*Hin*dIII fragments (∼600 bp) from the pBluescript derivatives were ligated into the expression vector pLcII (*24*), and the ligation products were introduced into *E. coli* strain M5219. Cell growth and protein purification were performed as described previously (*16*). After reconstitution with hemin, the WT, H64V, VH, VHA, and VHG proteins were digested with TPCK-treated trypsin (Sigma) to remove the N-terminal CII leader peptide. In the case of the VHAF and VHGF quadruple mutants, however, trypsin treatment resulted in overdigestion of the protein, and thus these mutants were purified as fusion proteins which retain the N-terminal leader sequence of 38 residues. Proteins were purified to homogeniety as judged by SDS polyacrylamide gel electrophoresis criteria. Mb concentrations were evaluated from the heme content, which was measured by a pyridine hemochrome assay.

Absorption Spectroscopy. The absorption spectra of the purified proteins were recorded on a Beckman DU640 spectrophotometer. Ferrous proteins were prepared by addition of solid sodium dithionite under nitrogen. Ferrous−CO-bound spectra were measured under 1 atm CO. pH titrations of the ferric proteins were performed in 10 mM sodium phosphate and 0.1 M NaCl. Aliquots of HCl or NaOH were added to solutions containing approximately 10 μM protein. The pH in the cuvette was monitored directly using a microelectrode (Hitachi). The proteins were also titrated with potassium cyanide in 10 mM sodium phosphate and 0.1 M NaCl (pH 7.0). The extent of formation of HCN at this pH was not calibrated, although the free cyanide concentration was calculated taking the amount of protein-bound cyanide into account.

Resonance Raman Spectroscopy. Spectra were recorded using a double monochromator (Jasco R-800) with a slit width of 6 cm^{-1}, following excitation by a krypton ion laser (406.7-nm line, Coherent I-302) with a laser power of 35 mW at the sample. A photomultiplier detector was used (Hamamatsu Photonics, R595), and the frequencies were calibrated with indene. A spinning Raman cell was used throughout the measurements. The samples contained 100 μM protein in buffers specified in the respective figure legends. Ferrous proteins were prepared by the addition of sodium dithionite, after purging extensively with nitrogen gas. The carbonmonoxy forms were prepared by the addition

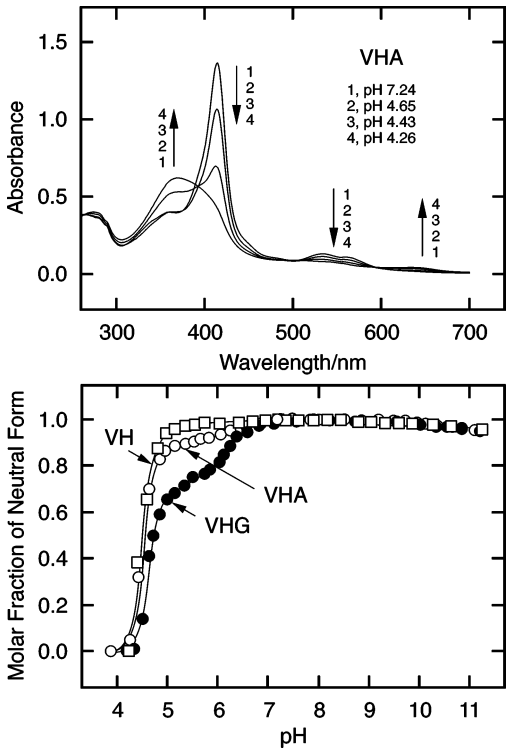

FIGURE 2: pH titration of the ferric double and triple mutants. Upper panel: absorption spectra of the VHA mutant at pH 7.24 (1), 4.65 (2), 4.43 (3), and 4.26 (4). The spectra were measured in 10 mM sodium phosphate and 0.1 M NaCl. Lower panel: the molar fraction of neutral form of VH (open squares), VHA (open circles), and VHG (closed circles) plotted against pH. The Soret maxima of the neutral Mbs around 415 nm were traced and normalized.

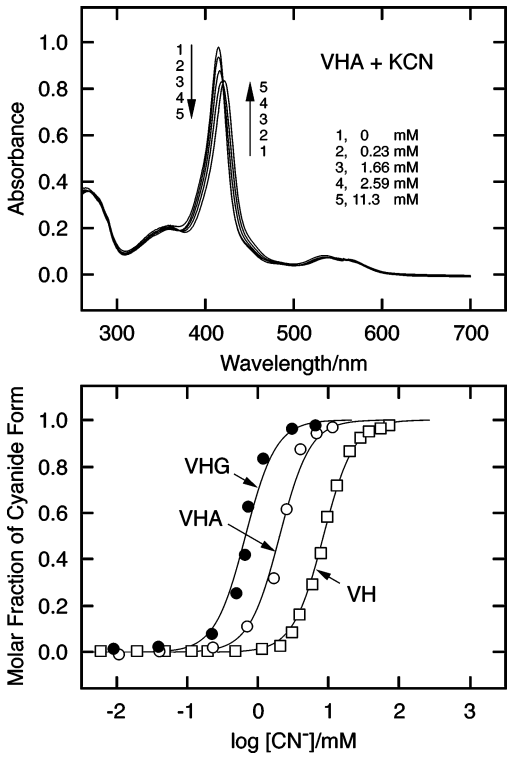

FIGURE 3: Cyanide titration of ferric double and triple mutants. Upper panel: absorption spectra of the VHA mutant in the presence of 0 (1), 0.23 (2), 1.66 (3), 2.59 (4), and 11.3 mM (5) potassium cyanide. The spectra were measured in 10 mM sodium phosphate and 0.1 M NaCl (pH 7.0). Lower panel: molar fraction of cyanide-bound VH (open squares), VHA (open circles), and VHG (closed circles) plotted against the logarithm of the cyanide concentration. The Soret maxima of the cyanide-free and bound Mbs were traced and normalized. The theoretical curves were drawn assuming 2 equiv of cyanide bind simultaneously to the heme.

of sodium dithionite under 1 atm CO. The spectra of the CO form were obtained with a defocused laser beam operating at 3 mW.

CO Binding Kinetics. CO association was monitored at 25 °C using a laser flash photolysis system (Unisoku) at the Graduate School of Engineering, Kyushu University. After photolysis of ferrous CO-bound Mb with a 5 ns pulse at 532 nm from a Continuum Q-switched Nd:YAG laser, ligand recombination was followed by monitoring absorbance changes at 423 nm. The experiments were performed with 10 μM Mbs in 10 mM sodium phosphate and 0.1 M NaCl (pH 7.0) under 1 atm of CO.

RESULTS

Absorption Spectra of the Triple Mutants. To construct a proximal heme pocket in Mb, we first replaced the axial His93 ligand of the VH double mutant by Gly (VHG) or Ala (VHA), which have less bulky side chains incapable of iron coordination. When axial ligands are removed from six-coordinated heme proteins, facile heme loss often occurs (*25*). Thus, we first studied the pH stability of the ferric triple mutants in order to establish whether heme is retained in these proteins. As seen in Figure 2 (upper), the VHA mutant shows a strong Soret absorption peak at 415 nm at neutral pH. This peak is replaced by a broad band around 370 nm at acidic pH. The latter band is characteristic of free hemin, indicating that an endogenous heme axial ligand provided by the protein matrix is lost as the pH is lowered. The molar fraction of the neutral form, calculated from the change in the Soret absorbance, is plotted against pH in Figure 2 (lower). The triple mutants showed no significant spectral changes between pH 7 and 11. VHG shows a small decrease in its Soret absorption between pH 6 and pH 5, a phenomenon also exhibited to a much smaller extent by VHA. The VH double mutant shows no such change and is stable even at pH 5. Thus, it is clear the triple mutants (i) retain heme at neutral and alkaline pH and (ii) have pH profiles distinct from that of the VH double mutant.

If a pocket has been created on the proximal side of the heme in the triple mutants, then it should accept an external ligand with moderate to high affinity. Thus, ligand binding to the VHA and VHG mutants was studied in cyanide titration experiments. The cyanide ion has high affinity for ferric hemes, and binding can be conveniently monitored by absorption spectroscopy.

As shown in Figure 3 (upper panel), the spectrum of VHA changes as the cyanide concentration is increased, with one set of isosbestic points being observed during the titration. Thus, binding appears to be a one-step process which can be described by a simple equilibrium between cyanide-free and bound states. The molar fraction of the cyanide-bound form can be estimated from the absorbance change at the Soret maximum (Figure 3, lower panel). Theoretical curves, drawn assuming that 2 equiv of cyanide bind to the heme in a highly cooperative manner, were able to reproduce the observed plots nicely. The free cyanide concentration needed to half-saturate the protein was estimated. It is clear that

Table 1: Absorption Maxima of the Double and Triple Mutants at pH 7.0

form	protein	soret/nm		visible/nm
ferric neutral	VHA	415	534	563
	VHG	414	533	562
	VH	412	526	632
ferric cyanide	VHA	422	541	
	VHG	422	543	
	VH	421	539	
ferrous	VHA	426	529	564
	VHG	427	530	564
	VH	426	529	563

cyanide binds with higher affinity to the triple mutants (K_d = 0.67 mM for VHG, 2.04 mM for VHA) than to the VH double mutant (8.51 mM), which may be attributable to the weaker axial coordination of the endogenous ligands in the triple mutants.

In Table 1, the absorption maxima of the double and triple mutants in the ferric, ferric−cyanide-bound, and ferrous states are summarized. The profile of the ferric neutral forms differs slightly between the double and triple mutants, suggesting distinct coordination structures. In contrast, the spectral profiles of the ferric-cyanide and ferrous forms are similar. If a pocket that can accommodate an exogenous ligand has been constructed, the ferrous triple mutants should show profiles distinct from that of the double mutant, which as we will show later is a six-coordinate low-spin species. Clearly they do not. A second puzzling observation is the much lower cyanide affinities of the triple mutants relative to WT Mb (1.87 μM). To probe the triple mutants further, their active site structures were investigated by resonance Raman spectroscopy.

Resonance Raman Spectra of the Triple Mutants. Resonance Raman spectroscopy is a powerful tool for probing heme structure, and the Raman lines in the frequency region between 1350 and 1650 cm^{-1} are sensitive to the porphyrin core size and to the oxidation state, spin state, and coordination number of the heme iron (*26*, *27*). Extensive analysis has allowed the most of the frequency modes in Mb to be assigned to specific stretching and bending of particular bonds or systems of bonds (*28*). Ferric VH Mb has been shown to be a six-coordinate species by X-ray crystallography (*18*) (Figure 1), and resonance Raman spectra support this structure (Figure 4). The ν_2, ν_{38}, ν_3, and ν_4 lines are observed at 1581, 1561, 1509, and 1373 cm^{-1}, respectively, and these frequencies are typical of six-coordinate ferric low-spin hemes and similar to those reported previously (*29*). In the case of the triple mutants VHA and VHG, these modes are observed at 1576, 1548, 1503, and 1373 cm^{-1}, respectively. These frequencies are again typical of six-coordinate ferric low-spin hemes, although the frequencies for the core-size markers (ν_2, ν_{38}, and ν_3) are substantially lower than those in the VH mutant. Thus, the porphyrin core seems to be somewhat expanded (*30*) in the triple mutants, even though a strong-field ligand (His68) is coordinating the ferric heme.

In Figure 5, resonance Raman spectra of the ferrous mutants are shown. In the spectrum of VH, the ν_2, ν_{38}, ν_3, and ν_4 lines are observed at 1586, 1557, 1494, and 1362 cm^{-1}, respectively, indicating the presence of a six-coordinate ferrous low-spin heme (*29*). This proposal is reasonable in

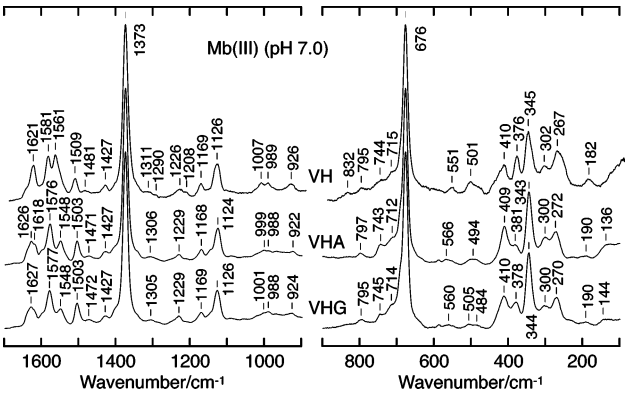

FIGURE 4: Resonance Raman spectra of the ferric double and triple mutants. From top: VH, VHA, and VHG. The samples contained 100 μM mutant proteins in 10 mM sodium phosphate buffer and 0.1 M NaCl (pH 7.0). Spectral condition: slit width, 6 cm^{-1}; laser, 406.7 nm at 35 mW.

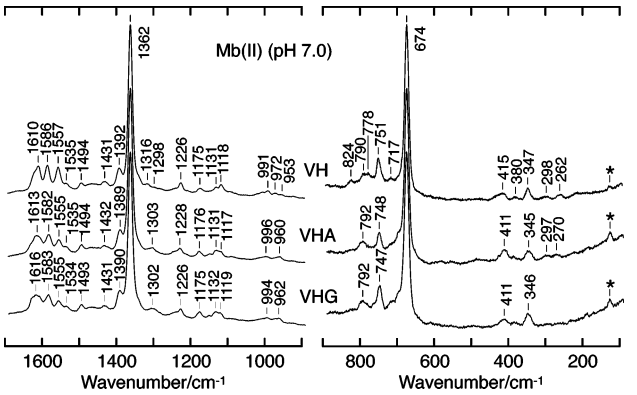

FIGURE 5: Resonance Raman spectra of the ferrous double and triple mutants. From top: VH, VHA, and VHG. The samples contained 100 μM mutant proteins in 10 mM sodium phosphate buffer and 0.1 M NaCl (pH 7.0). Spectral condition: slit width, 6 cm^{-1}; laser, 406.7 nm at 35 mW. Asterisks indicate plasma line of the krypton laser.

the light of the VH crystal structure, which showed a six-coordinate ferric heme (*18*) (Figure 1), the two axial ligands being His68 and His93. In the triple mutants, the corresponding Raman lines are observed at 1582, 1555, 1494, and 1362 cm^{-1}, respectively, and the spectral profiles in the high and low-frequency regions are essentially the same as that of the double mutant ie with a six-coordinate low-spin ferrous heme. Thus, it is clear that the proximal coordination site of the heme is occupied by a strong field ligand in both the ferric and ferrous forms of the triple mutants.

It is curious that a second strong-field ligand is coordinating the heme, given that His93 of VH has been replaced in the triple mutants. Inspecting the proximal pocket in the crystal structure of the VH mutant for clues as to the nature of the unidentified ligand, no candidate other than His97 suggested itself (Figure 1). This residue is located at the first position of the FG corner (FG1), one helical turn from the proximal ligand His93 (F8). The Cβ atom of His97 is situated 6.17 Å from the heme iron, a distance which compares well with that between Cβ of His93 and the iron (5.77 Å) (*18*). Although the imidazole ring of the His97 is close to parallel to the heme plane and interacting with the heme propionate in the VH mutant, spatial rearrangements of proximal pocket residues may allow the His97 side chain to form a bond to the iron in the triple mutants. To examine this possibility,

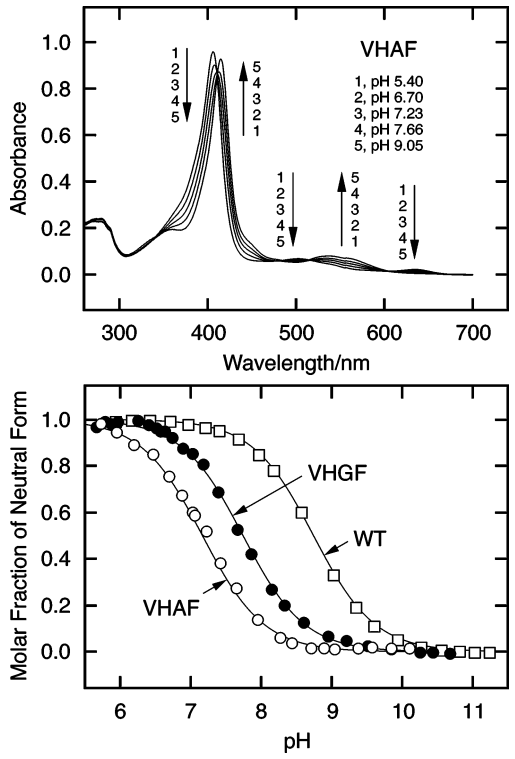

FIGURE 6: pH titration of ferric quadruple mutants and WT Mb. Upper panel: absorption spectra of the VHAF mutant at pH 5.40 (1), 6.70 (2), 7.23 (3), 7.66 (4), and 9.05 (5). The spectra were measured in 10 mM sodium phosphate and 0.1 M NaCl. Lower panel: molar fraction of neutral form of WT (open squares), VHAF (open circles), and VHGF (closed circles) plotted against pH. The Soret maxima of the neutral Mbs at about 407 nm were traced and normalized. The theoretical curves were drawn assuming an equilibrium in which one proton equivalent is involved..

we constructed the quadruple mutants VHAF and VHGF in which His97 is replaced by Phe. This is a conservative substitution since both His and Phe have aromatic and planar side chains, though of course the Phe side chain is incapable of coordinating the iron. The single mutation of His97 to Phe has been reported to have only small effects on heme stability and oxygen binding (*31*, *32*).

Absorption Spectra of the Quadruple Mutants. As seen in Figure 6 (upper panel), the absorption spectrum of the ferric VHAF quadruple mutant is pH sensitive in the range pH 7−11. Since one set of isosbestic points was observed for both quadruple mutants, the titration curves were analyzed in terms of a simple equilibrium between the neutral and alkaline forms of the proteins. The absorbance changes at the Soret maxima of the two forms were normalized, and the molar fraction of the neutral form was plotted against the pH in Figure 6 (lower panel). For comparison, the pH profile of the WT protein was measured and displayed in the same panel. Theoretical curves drawn assuming that the alkaline transition (H_2O/OH^-) involves one proton equivalent provide a satisfactory fit to the titration data. The apparent pK_a values of the alkaline transition in VHAF and VHGF were calculated to be 7.17 and 7.74, respectively, lower than that of the WT protein (pK_a = 8.74). This pH-dependent behavior of the quadruple mutants is distinct from that of the triple mutants (Figure 2), indicating unequivocally that His97 in the triple mutants is the second strong-field ligand.

The absorption maxima of the quadruple mutants are compared with those of the WT protein in Table 2. The

Table 2: Absorption Maxima (nm) of the WT and Quadruple Mutant Mbs

form	protein	soret/nm		visible/nm
ferric neutral[a]	VHAF	406	503	635
	VHGF	407	503	635
	WT	408	503	631
ferric alkaline[b]	VHAF	415	537	557
	VHGF	415	539	557
	WT	413	542	582
ferric cyanide[c]	VHAF	422	542	
	VHGF	422	542	
	WT	423	541	
ferrous[c]	VHAF	433	560	
	VHGF	434	559	
	WT	433	556	
ferrous CO[c]	VHAF	423	542	572
	VHGF	423	542	571
	WT	422	541	578

[a] At pH 6.0. [b] At pH 10.5. [c] At pH 7.0.

spectra of the ferric neutral forms of these proteins are very similar to one another. This suggests that the heme coordination structure is common in these proteins. In WT pig Mb at neutral pH, a water molecule is the sixth ligand of the heme, as shown by X-ray crystallography (*13*). The alkaline transition has been investigated in ferric Mb from many different species, and it is established that the dissociation of one proton equivalent converts a water ligand to a hydroxide ligand at alkaline pH (*33*). The spectral similarity of the quadruple mutants and WT Mb and their common pH behavior suggest strongly that both have similar axial ligands in the ferric state.

To examine the accessibility of the proximal heme pocket to exogenous ligands, cyanide binding to the quadruple mutants was investigated. As shown in Figure 7 (upper), the absorption spectrum of theVHAF mutant changed with a single set of isosbestic points on increasing the cyanide concentration. The weak absorption band around 630 nm decreased, which suggests that the iron changes from a high- to a low-spin state. Again, cyanide binding was analyzed in terms of a simple one-step equilibrium, and the molar fractions of the cyanide-bound proteins are plotted against the logarithm of the free cyanide concentration in Figure 7 (lower). Both quadruple mutants show similar titration profiles, and the dissociation constants for cyanide (K_d) were calculated to be 5.85 μM (VHAF) and 5.65 μM (VHGF), which are close to that of WT Mb (1.87 μM). These values are about 2 orders of magnitude smaller than those of the triple mutants and some 10-fold lower than that of the H64V mutant (64.6 μM, Figure 7). Thus, it is clear that the His97-to-Phe mutation allows exogenous ligands to bind to the heme with affinities comparable to the WT protein.

Resonance Raman Spectra of Quadruple Mutants. The active site structure of the quadruple mutants was studied by resonance Raman spectroscopy. In Figure 8, spectra of the neutral forms of the ferric proteins are compared. In the spectra of the quadruple mutants, the ν_2, ν_{38}, ν_3, and ν_4 lines at 1560, 1513, 1483, and 1371 cm^{-1}, respectively, are very similar to those of the WT protein (1564, 1514, 1482, and 1372 cm^{-1}), indicating the presence of six-coordinate ferric high-spin heme. This structure is consistent with water coordination in these three proteins as suggested by the pH titration data (Figure 6). At alkaline pH, however, the

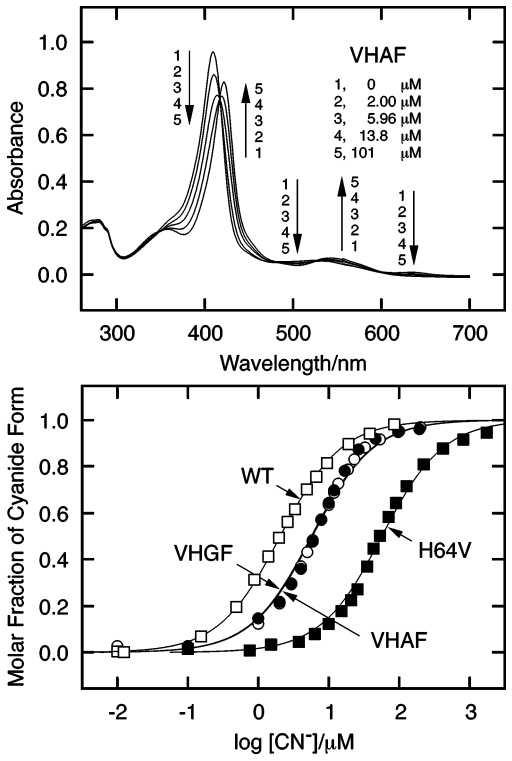

FIGURE 7: Cyanide titration of ferric quadruple mutants and WT Mb. Upper panel: absorption spectra of the VHAF mutant in the presence of 0 (1), 2.00 (2), 5.96 (3), 13.8 (4), and 101 μM (5) potassium cyanide. The spectra were measured in 10 mM sodium phosphate and 0.1 M NaCl (pH 7.0). Lower panel: molar fraction of cyanide-bound WT (open squares), VHAF (open circles), and VHGF (closed circles) plotted against the logarithm of the cyanide concentration. The Soret maxima of the cyanide-free and bound Mbs were traced and normalized. The theoretical curves were drawn assuming one equivalent of cyanide binds to the heme.

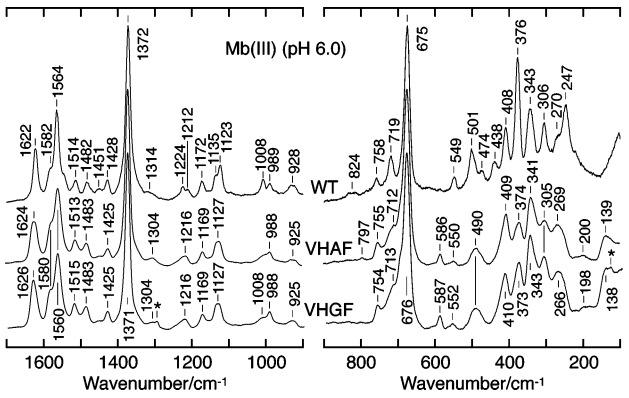

FIGURE 8: Resonance Raman spectra of the ferric quadruple mutants and WT Mb. From top: WT, VHAF, and VHGF. The samples contained 100 μM proteins in 10 mM sodium phosphate buffer and 0.1 M NaCl (pH 6.0). Spectral condition: slit width, 6 cm^{-1}; laser, 406.7 nm at 35 mW. Asterisks indicate plasma lines of the krypton laser.

quadruple mutants showed different spectral properties to the WT protein (Figure 9). The quadruple mutants exhibit ν_2, ν_3, and ν_4 lines at 1576, 1503, and 1373 cm^{-1}, respectively, in contrast to the corresponding lines in the WT protein at 1565, 1482, and 1375 cm^{-1}. The ν_2 and ν_3 frequencies of the quadruple mutants are substantially higher and indicate the presence of six-coordinate low-spin heme. The spectral profiles of the alkaline forms of the quadruple mutants more closely resemble those of the triple mutants

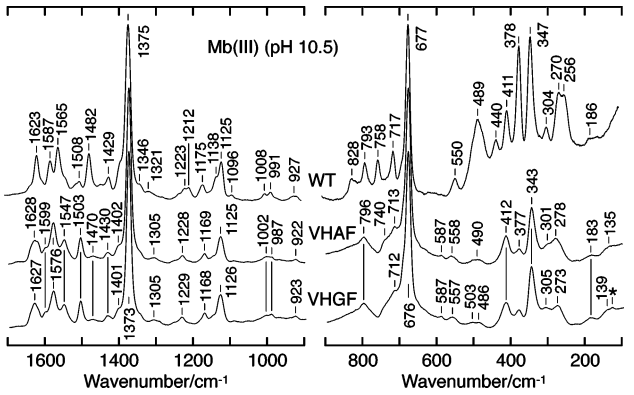

FIGURE 9: Resonance Raman spectra of the ferric quadruple mutants and WT Mb at alkaline pH. From top: WT, VHAF, and VHGF. The samples contained 100 μM proteins in 100 mM sodium phosphate (pH 10.5). Spectral condition: slit width, 6 cm^{-1}; laser, 406.7 nm at 35 mW.

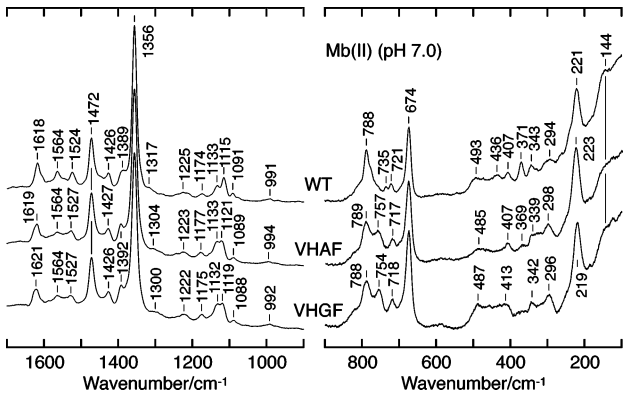

FIGURE 10: Resonance Raman spectra of the ferrous quadruple mutants and WT Mb. From top: WT, VHAF, and VHGF. The samples contained 100 μM mutant proteins in 10 mM sodium phosphate and 0.1 M NaCl (pH 7.0). Spectral condition: slit width, 6 cm^{-1}; laser, 406.7 nm at 35 mW.

at neutral pH (Figure 4) than they do those of the WT protein at alkaline pH (Figure 9). The absorption spectral profiles (Tables 1 and 2) further emphasize the similarity between the alkaline forms of the quadruple and the neutral forms of the triple mutants. These spectral similarities suggest that the quadruple mutants at alkaline pH and the triple mutants at neutral pH share a common hydroxide ligand.

In the ferrous state, the resonance Raman profiles of the quadruple mutants are similar to the WT protein, each exhibiting lines at about 1564 (ν_2), 1527 (ν_{38}), 1472 (ν_3), and 1356 cm^{-1} (ν_4) (Figure 10). These frequencies indicate that five-coordinate ferrous high-spin hemes are contained in these proteins. The profiles differ markedly from those of the triple mutants (Figure 5), consistent with the mutation of His97 to Phe leading to a loss of proximal axial ligation in the ferrous state. In the lower-frequency region, the WT protein exhibits a line at 221 cm^{-1}, which may be assigned to the ν(Fe−His) stretching mode (*34*, *35*). Both quadruple mutants show similar lines at about 220 cm^{-1}, suggesting strongly that the sole axial ligand in these mutants is His68. These data establish that the quadruple mutations create a proximal heme pocket in the ferric as well as the ferrous states.

The environment of the ligand binding pocket was next examined with a CO probe (Figure 11). The ν(Fe−CO) and

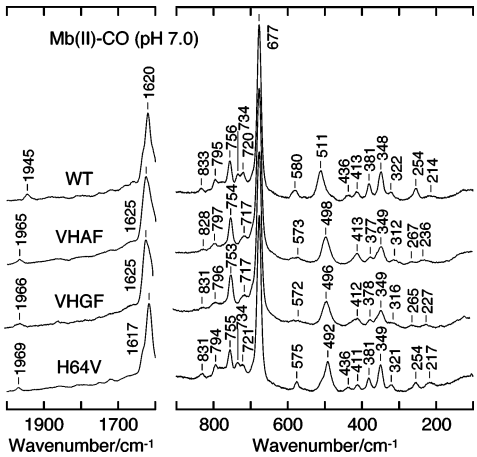

FIGURE 11: Resonance Raman spectra of ferrous-CO bound VHGF, VHAF, VH, and WT Mb. The samples contained 100 μM proteins in 10 mM sodium phosphate and 0.1 M NaCl (pH 7.0). Spectral condition: slit width, 6 cm^{-1}; laser, 406.7 nm at 3 mW with defocused laser beam.

Table 3: Rate Constants for CO Binding to Porcine Mb

protein	$k'_{on}/\mu M^{-1}\,s^{-1}$	ref
WT	0.78	18
H64V	5.4	18
VH	0.10	18
VHA[a]	0.15	this work
VHAF	13	this work

[a] Biphasic kinetics were observed, and the slower rate constant is depicted.

ν(C−O) stretching frequencies have been shown to be inversely proportional to one another, and to be sensitive to the polarity of the environment around the bound CO (*36*−*40*). In the WT protein, the Raman line at 511 cm^{-1} can be assigned to the ν(Fe−CO) stretching mode, its frequency being similar to that of sperm whale Mb (512 cm^{-1}) (*41*). The weak line at 580 cm^{-1} is close to the δ(Fe−C−O) bending frequency (577 cm^{-1}) (*41*) of sperm whale Mb. In addition, a weak but apparent line at 1945 cm^{-1} can be assigned to the ν(C−O) stretching mode, and this mode was observed at 1944 cm^{-1} in WT pig Mb in an IR study (*42*). In the quadruple mutants, lines for the ν(Fe−CO) and ν(C−O) stretches are observed at about 500 and 1965 cm^{-1}, respectively. These frequencies are close to the corresponding frequencies in H64V Mb (492 and 1969 cm^{-1}). The δ(Fe−C−O) line is poorly resolved in the quadruple mutants. The ν(Fe−CO) frequency is lower than that of the WT protein while the ν(C−O) stretch is higher, and this ν(Fe−CO)/ν(C−O) frequency pair strongly suggests that in the quadruple mutants, the CO is bound in a more hydrophobic environment than in the WT protein, possibly because the side chain of Phe97 is situated close to the CO ligand.

Further evidence for a hydrophobic proximal pocket environment is provided from measurements of the rate constants of CO association to the ferrous proteins (Table 3). For VHAF, the on rate (k'_{CO}) is 16-fold larger than that of WT Mb and closer to that for H64V mutant. The large k'_{CO} value suggests that the distal pocket water molecule stabilized by the distal His64 and whose displacement presents a kinetic barrier to ligand binding in WT Mb (*4*), is removed in the VHAF mutant. The VHA mutant showed biphasic absorbance changes after CO photolysis, and the smaller k'_{CO} (0.15 $\mu M^{-1}s^{-1}$) is similar to that of VH (0.10 $\mu M^{-1}s^{-1}$) (*18*). This supports the idea that the heme iron in ferrous VHA is coordinated by two His residues, as it is in the VH mutant. The faster phase (half-life 28 μs) probably corresponds to the rebinding of the endogenous His to the iron after photolysis, since biphasic binding processes have been reported for neuroglobin (*43*−*45*) and cytoglobin (*46*), both of which have His/His coordination. The biphasic process has not been reported for VH (*18*), and this difference may be attributable to the weak and slow His68 coordination in the VH mutant. In other words, His68/His97 coordination in the VHA mutant is tighter than the His68/His93 counterpart in the VH mutant in the ferrous state.

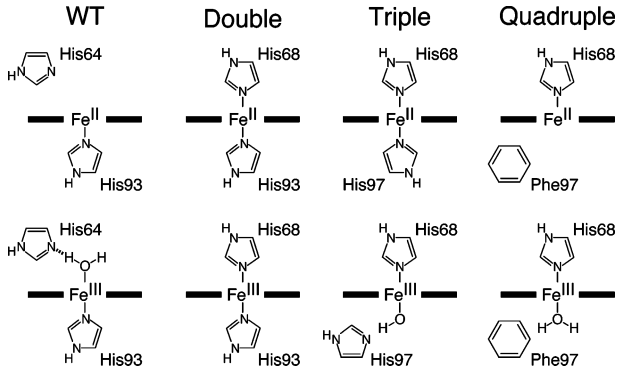

FIGURE 12: Schematic drawing of the heme ligands in the WT, double, triple, and quadruple mutant Mbs. Upper row; ferrous proteins: lower row; ferric proteins.

DISCUSSION

Coordination Structure. A proximal heme pocket has been engineered within the framework of the Mb scaffold, starting from the bis-histidine coordinated VH double mutant. The proposed ligation states in the various Mb forms examined in this work are summarized schematically in Figure 12. The VH mutant has six-coordinate low-spin heme in both its ferric (Figure 4) and ferrous (Figure 5) states. This structure is consistent with His68 and His93 coordination, as revealed earlier by X-ray crystallography (*18*). The heme was unexpectedly found to be six-coordinate in the ferrous forms of the triple mutants, in which the His93 ligand is replaced by Gly or Ala (Figure 5). The proximal ligand was established to be His97, since replacement of this residue by Phe resulted in a five-coordinate heme (Figure 10). The Raman profiles, as well as the absorption profiles (Table 1), of the ferrous triple mutants resemble that of the VH mutant, consistent with similar His/His coordination (Figure 12).

In contrast, the ferrous quadruple mutants were found to contain five-coordinate high-spin heme, the sole axial ligand being His68 as indicated by (i) the observed ν(Fe−His) stretching frequency (Figure 10) and (ii) the similarity of the absorption spectra of the quadruple mutants and the WT protein (Table 2). The Fe−His68 bond is strained in the VH mutant (Figure 1), and we might expect this bond to be strained in the quadruple mutants, if the coordination geometry is unchanged. In the ferrous quadruple mutants, however, the ν(Fe−His) stretching frequency is similar to that in the WT protein (ca. 220 cm^{-1}). Since a similar stretching frequency is expected to reflect a similar bond strength, the strain in the VH mutant may have been relieved by the quadruple mutation.

The ferric quadruple mutants show pH-dependent spectral changes similar to the WT protein (Figure 6). In the WT protein, the pH dependence arises from deprotonation of the coordinated water molecule in the distal pocket at alkaline pH, and this process is inhibited by the distal His64 (*33*). In the quadruple mutants, there is no such histidine on the proximal side of the heme since His97 has been replaced by Phe. Thus, the pH-dependent spectral changes in the quadruple mutants may reflect direct dissociation of a proton from a liganded water bound at the proximal coordination site. The observed pK_a is close to that of free hemin in water (pK_a = 7.1) (*47*) or water-soluble iron−porphyrins (pK_a = 7.24) (*48*). The pK_a value of VHAF is lower than that of VHGF, probably reflecting the ease of access of a hydroxide anion to the heme pocket. By contrast, the higher pK_a of WT Mb arises because the distal His64 stabilizes bound water ligands by hydrogen bond formation, thereby inhibiting the dissociation of a proton from water to give hydroxide.

This interpretation accounts for the observation of low-spin ferric heme in the alkaline form of the quadruple mutants. In the alkaline WT protein, the heme is in a mixed-spin state even though hydroxide coordination has been established (*33*). This is because the distal His64 donates a hydrogen bond to the hydroxide ligand, thereby weakening the Fe−OH bond. In the quadruple mutants, there are no nearby groups capable of proton donation and the hydroxide acts as a strong-field ligand. We were unable to detect the ν(Fe−OH) line, which is expected to be weak (*49*), in the Raman spectrum. The alkaline form of ferric horseradish peroxidase, which also contains a low-spin heme, has been shown to have histidine and hydroxide at the axial coordination sites (*50*). Thus, we conclude that hydroxide has a strong ligand-field effect, which can be diminished by hydrogen bond donation from nearby residues such as His64 in WT Mb.

The resonance Raman profiles (Figures 4 and 9) and absorption spectra (Tables 1 and 2) of the ferric triple mutants are quite similar to those of the alkaline forms of the quadruple mutants, again indicating hydroxide anion coordination. As an anion, hydroxide will neutralize the ferric heme in the triple mutants. In the ferrous state, the iron does not require a balancing negative charge, and coordination to the neutral His97 ligand is favored. It should be noted here that a cavity-forming mutant of Mb, H93G, has been shown to have hydroxide as the sole ligand at alkaline pH (*51*), and it has been suggested that the hydroxide is bound in the proximal nonpolar pocket. Our triple mutant results also suggest hydroxide ligand coordination from the proximal side (*51*), although here the distal coordination site is occupied by His68 (Figure 12).

Heme Pocket. At this point, it would be useful to consider why four mutations are needed to construct a proximal heme pocket in which exogenous ligands can bind. Comparing the ferric quadruple and triple mutants, it is evident that His97 is the key determinant of hydroxide coordination. In contrast to the VH double mutant, the spectral characteristics of the ferric triple mutants are pH-dependent, with small absorbance decreases occurring around pH 6 (Figure 2). These spectral changes may reflect the protonation of His97. The His97 imidazole group lies parallel to the porphyrin in crystal structures of Mb (e.g., Figure 1) with one edge located close to the axial coordination site and another edge oriented toward the solvent and the heme-7-propionate. Thus, this residue is well placed to stabilize bound hydroxide. The hydroxide ligand in the triple mutants may donate less electrons to the iron than the histidine ligand in the VH double mutant, and the resultant weaker ligation may account for the expanded porphyrin core in the former (Figure 4). The weaker coordination of hydroxide in the triple mutants relative to the imidazole of His93 in the VH mutant would also explain the higher cyanide affinity of the triple mutants. Comparing the titration curves in Figures 3 and 7, it is clear that two cyanide molecules bind simultaneously to the ferric heme in the double and triple mutants. The strongly coordinating hydroxide or His93 inhibit the binding of the first cyanide ligand, and the dissociation of the strained His68 in the double and triple mutants triggers the simultaneous binding of two cyanides.

The cyanide affinity increases by 2 orders of magnitude, to a value comparable with that of the WT protein, upon replacement of His97 by Phe in creating the quadruple mutants. Weak water coordination is the main reason for the large increase in the cyanide affinity of the quadruple mutants. Cyanide affinity in myoglobin has been shown to depend on the ease of displacement of coordinated water as well as the acid dissociation constant of HCN inside the protein (*52*, *53*). The frequencies of the CO vibrational modes (Figure 11) and the CO association rates (Table 3) suggest that the proximal heme pocket in the quadruple mutants has a similar polarity to that of the distal pocket in the H64V single mutant, even though the cyanide affinity is almost an order of magnitude lower in the latter (Figure 7). In addition, the pK_a of the water ligand differs by more than one unit between the quadruple mutants and WT Mb. Thus, it appears that the proximal heme pocket presents a ligand binding environment quite different in polarity to that in the distal pocket of the WT protein.

Reaction of the triple and quadruple mutants with air, after reduction with sodium dithionite, resulted in a rapid oxidation of the iron, and we were unable to measure spectra of the oxy form or measure the rate of autoxidation using a conventional spectrometer with a mixing time of ~10 s. Similar problems were encountered with the VH double mutant (*18*). An unstable oxy form is not surprising since there are no nearby polar residues available to stabilize bound O_2 in the way that the distal His64 does in WT Mb. The rapid oxidation rates may suggest that the proximal side of the heme has an open structure, allowing easy access of water to the heme and facilitating autoxidation (*54*).

In summary, we have been able to engineer a pocket on the proximal side of the heme in Mb. The cyanide affinity and pH titration behavior of the mutant proteins are quite similar to those of the WT protein, although the polarities of the respective proximal and distal pockets are distinct. The stable ligand binding pocket on the proximal face of the heme may serve as a framework onto which further functional groups may be introduced with a view to engineering redox-linked chemistry at the heme.

ACKNOWLEDGMENT

We thank Dr. Takashi Hayashi and Dr. Hideaki Sato, Graduate School of Engineering, Kyushu University, Japan,

for the measurements of CO binding kinetics and helpful discussion.

REFERENCES

1. Springer, B. A., and Sligar, S. G. (1987) *Proc. Natl. Acad. Sci. U.S.A. 84*, 8961−8965.
2. Varadarajan, R., Szabo, A., and Boxer, S. (1985) *Proc. Natl. Acad. Sci. U.S.A. 82*, 5681−5684.
3. Dodson, G., Hubbard, R. E., Oldfield, T. J., Smerdon, S. J., and Wilkinson, A. J. (1988) *Protein Eng. 2*, 233−237.
4. Springer, B. A., Sligar, S. G., Olson, J. S., and Phillips, G. N., Jr. (1994) *Chem. Rev. 94*, 699−714.
5. Lesk, A. M., and Chothia, C. (1980) *J. Mol. Biol. 136*, 225−270.
6. Bashford, D., Chothia, C., and Lesk, A. M. (1987) *J. Mol. Biol. 196*, 199−216.
7. Phillips, S. E., and Schoenborn, B. P. (1981) *Nature 292*, 81−82.
8. Hanson, J. C., and Schoenborn, B. P. (1981) *J. Mol. Biol. 153*, 117−146.
9. Springer, B. A., Egeberg, K. D., Sligar, S. G., Rohlfs, R. J., Mathews, A. J., and Olson, J. S. (1989) *J. Biol. Chem. 264*, 3057−3060.
10. Bunn, H. F., and Forget, B. G. (1986) in *Hemoglobin: Molecular, Genetic, and Clinical Aspects*, pp 634−662, W. B. Saunders Co., Philadelphia.
11. Hargrove, M. S., Singleton, E. W., Quillin, M. L., Ortiz, L. A., Phillips, G. N., Olson, J. S., and Mathews, A. J. (1994) *J. Biol. Chem. 269*, 4207−4214.
12. Quillin, M. L., Arduini, R. M., Olson, J. S., and Phillips, G. N., Jr. (1993) *J. Mol. Biol. 234*, 140−155.
13. Oldfield, T. J., Smerdon, S. J., Dauter, Z., Petratos, K., Wilson, K. S., and Wilkinson, A. J. (1992) *Biochemistry 31*, 8732−8739.
14. Smerdon, S. J., Krzywda, S., Brzozowski, A. M., Davies, G. J., Wilkinson, A. J., Brancaccio, A., Cutruzzloa, F., Allocatelli, C. T., Brunori, M., Li, T., Brantley, R. E., Jr., Carver, T. E., Eich, R. F., Singleton, E. E., and Olson, J. S. (1995) *Biochemistry 34*, 8715−8725.
15. Conti, E., Moser, C., Rizzi, M., Mattevi, A., Lionetti, C., Coda, A., Ascenzi, P., Brunori, M., and Bolognesi, M. (1993) *J. Mol. Biol. 233*, 498−508.
16. Smerdon, S. J., Dodson, G. G., Wilkinson, A. J., Gibson, Q. H., Blackmore, R. S., Carver, T. E., and Olson, J. S. (1991) *Biochemistry 30*, 6252−6260.
17. Qin, J., La Mar, G. N., Dou, Y., Admiraal, S. J., and Ikeda-Saito, M. (1994) *J. Biol. Chem. 269*, 1083−1090.
18. Dou, Y., Admiraal, S. J., Ikeda-Saito, M., Krzywda, S., Wilkinson, A. J., Li, T., Olson, J. S., Prince, R. C., Pickering, I. J., and George, G. N. (1995) *J. Biol. Chem. 270*, 15993−16001.
19. Barrick, D. (1994) *Biochemistry 33*, 6546−6554.
20. DePillis, G. D., Decatur, S. M., Barrick, D., and Boxer, S. G. (1994) *J. Am. Chem. Soc. 116*, 6981−6982.
21. Decatur, S. M., and Boxer, S. G. (1995) *Biochemistry 34*, 2122−2129.
22. Roach, M. P., Pond, A. E., Thomas, M. R., Boxer, S. G., and Dawson, J. H. (1999) *J. Am. Chem. Soc. 121*, 12088−12093.
23. Hargrove, M. S., and Olson, J. S. (1996) *Biochemistry 35*, 11310−11318.
24. Nagai, K., and Thogersen, H. C. (1984) *Nature 309*, 810−812.
25. Uno, T., Yukinari, A., Moriyama, Y., Ishikawa, Y., Tomisugi, Y., Brannigan, J. A., and Wilkinson, A. J. (2001) *J. Am. Chem. Soc. 123*, 512−513.
26. Spiro, T. G., and Li, X.-Y. (1988) in *Biological Applications of Raman Spectroscopy* (Spiro, T. G., Ed.) Vol. 3, pp 1−38, Wiley-Interscience, New York.
27. Kincaid, J. R. (2000) in *The Porphyrin Handbook* (Kadish, K. M., Smith, K. M., and Guilard, R., Eds.) Vol. 7, pp 227−291, Academic Press, San Diego.
28. Hu, S., Smith, K. M., and Spiro, T. G. (1996) *J. Am. Chem. Soc. 118*, 12638−12646.
29. Anderton, C. L., Hester, R. E., and Moore, J. N. (1995) *Biochim. Biophys. Acta 1253*, 1−4.
30. Parthasarathi, N., Hansen, C., Yamaguchi, S., and Spiro, T. G. (1987) *J. Am. Chem. Soc. 109*, 3865−3871.
31. Hargrove, M. S., Wilkinson, A. J., and Olson, J. S. *Biochemistry* (1996) *35*, 11300−11309.
32. Liong, E. C., Dou, Y., Scott, E. E., Olson, J. S., and Phillips, G. N., Jr. *J. Biol. Chem.* (2001) *276*, 9093−9100.
33. Iizuka, T., and Yonetani, T. (1970) *Adv. Biophys. 1*, 157−182.
34. Kitagawa, T., Nagai, K., and Tsubaki, M. (1979) *FEBS Lett. 104*, 376−378.
35. Argade, P. V., Sassaroli, M., Rousseau, D. L., Inubushi, T., Ikeda-Saito, M., and Lapidot, A. (1984) *J. Am. Chem. Soc. 106*, 6593−6596.
36. Uno, T., Nishimura, Y., Tsuboi, M., Makino, R., Iizuka, T., and Ishimura, Y. (1987) *J. Biol. Chem. 262*, 4549−4556.
37. Li, T., Quillin, M. L., Phillips, G. N., Jr., and Olson, J. S. (1994) *Biochemistry 33*, 1433−1446.
38. Ray, G. B., Li, X.-Y., Ibers, J. A., Sessler, J. L., and Spiro, T. G. (1994) *J. Am. Chem. Soc. 116*, 162−176.
39. Oldfield, E., Guo, K., Augspurger, J. D., and Dykstra, C. E. (1991) *J. Am. Chem. Soc. 113*, 7537−7541.
40. Yu, N.-T., Kerr, E. A., Ward, B., and Chang, C. K. (1983) *Biochemistry 22*, 4534−4540.
41. Tsubaki, M., Srivastava, R. B., and Yu, N.-T. (1982) *Biochemistry 21*, 1132−1140.
42. Cameron, A. D., Smerdon, S. J., Wilkinson, A. J., Habash, J., Helliwell, J. R., Li, T., and Olson, J. S. (1993) *Biochemistry 32*, 13061−13070.
43. Kriegl, J. M., Bhattacharyya, A. J., Nienhaus, K., Deng, P., Minkow, O., and Nienhaus, G. U. (2002) *Proc. Natl. Acad. Sci. U.S.A. 99*, 7992−7997.
44. Dewilde, S., Kiger, L., Burmester, T., Hankeln, T., Baudin-Creuza, V., Aerts, T., Marden, M. C., Caubergs, R., and Moens, L. (2001) *J. Biol. Chem. 276*, 38949−38955.
45. Trent, J. T., III, Watts, R. A., and Hargrove, M. S. (2001) *J. Biol. Chem. 276*, 30106−30110.
46. Sawai, H., Kawada, N., Yoshizato, K., Nakajima, H., Aono, S., and Shiro, Y. (2003) *Biochemistry 42*, 5133−5142.
47. Uno, T., Takeda, A., and Shimabayashi, S. (1995) *Inorg. Chem. 34*, 1599−1607.
48. Zipplies, M. F., Lee, W. A., and Bruice, T. C. (1986) *J. Am. Chem. Soc. 108*, 4433−4445.
49. Feis, A., Marzocchi, M. P., Paoli, M., and Smulevich, G. *Biochemistry* (1994) *33*, 4577−4583.
50. Sitter, A. J., Shifflett, J. R., and Terner, J. (1988) *J. Biol. Chem. 263*, 13032−13038.
51. Das, T. K., Franzen, S., Pond, A., Dawson, J. H., and Rousseau, D. L. (1999) *Inorg. Chem. 38*, 1952−1953.
52. Brancaccio, A., Cutruzzola, F., Allocatelli, C. T., Brunori, M., Smerdon, S. J., Wilkinson, A. J., Dou, Y., Keenan, D., Ikeda-Saito. M., Brantley, R. E., Jr., and Olson, J. S. (1994) *J. Biol. Chem. 269*, 13843−13853.
53. Dou, Y., Olson, J. S., Wilkinson, A. J., and Ikeda-Saito, M. (1996) *Biochemistry 35*, 7107−7113.
54. Brantley, R. E., Jr., Smerdon, S. J., Wilkinson, A. J., Singleton, E. W., and Olson, J. S. (1993) *J. Biol. Chem. 268*, 6995−7010.

BI034569Z